

PCCP

Accepted Manuscript



This is an *Accepted Manuscript*, which has been through the Royal Society of Chemistry peer review process and has been accepted for publication.

Accepted Manuscripts are published online shortly after acceptance, before technical editing, formatting and proof reading. Using this free service, authors can make their results available to the community, in citable form, before we publish the edited article. We will replace this *Accepted Manuscript* with the edited and formatted *Advance Article* as soon as it is available.

You can find more information about *Accepted Manuscripts* in the [Information for Authors](#).

Please note that technical editing may introduce minor changes to the text and/or graphics, which may alter content. The journal's standard [Terms & Conditions](#) and the [Ethical guidelines](#) still apply. In no event shall the Royal Society of Chemistry be held responsible for any errors or omissions in this *Accepted Manuscript* or any consequences arising from the use of any information it contains.

Optical Properties of PbS Nanocrystal Quantum Dots at Ambient and Elevated Pressure

Kaifu Bian^a, Benjamin T. Richards^b, Hanqing Yang^a, William Bassett^c, Frank W. Wise^d,

Zhongwu Wang^e and Tobias Hanrath^{a}*

^aSchool of Chemical and Biomolecular Engineering, ^bDepartment of Materials Science and Engineering, ^c Department of Earth and Atmospheric Sciences, ^dSchool of Applied and Engineering Physics, ^eCornell High Energy Synchrotron Source (CHESS), Cornell University, Ithaca, NY, 14853

*Corresponding Author: Tobias Hanrath, th358@cornell.edu

KEYWORDS: nanocrystals, high-pressure, optical properties, phase transitions

Abstract

We investigated pressure-dependent changes in the optical properties of PbS nanocrystal quantum dots (NQD) by combining X-ray scattering and optical absorption spectroscopy in a diamond anvil cell. We discovered that the excitonic absorption peak vanishes as the NQD crystal structure reversibly undergoes the pressure-induced phase transition from rock-salt to orthorhombic structure. In the rock-salt phase, the pressure coefficient $\frac{\partial E_g}{\partial P}$ of PbS NQD is negative and decreases in magnitude with decreasing NQD size. The basic theoretical model based on literature values of the PbS bulk modulus significantly overestimated the change in pressure coefficient with NQD size. We present a model that includes the size-dependence of both the pressure coefficient and bulk modulus to describe the experimentally observed optical and structural trends.

Introduction

Recent advances in the synthesis, characterization and emerging understanding of size-dependent properties of semiconductor nanomaterials have created many opportunities for potentially transformative advances in the field of electronic and optical materials. Semiconductor nanocrystal quantum dots (NQDs), in particular, have captivated the field as a material with potential major impact for a broad range of technologies.¹⁻⁶ Among the growing library of semiconductor nanomaterials that has emerged from the recent surge of interest in the field, lead salt (PbX; X=S,Se,Te) NQDs stand out as a fundamentally intriguing and experimentally advantageous system for several reasons. PbX NQDs are among the most strongly quantum confined systems by virtue of the large Bohr radius of the exciton (~20 nm in PbS). Adjusting the NQD diameter between 2 and 10 nm provides an experimentally tunable energy gap ranging from 0.4 to nearly 2 eV. Colloidal PbX NQDs can be readily prepared with ~5-10% relative size distribution, which has enabled rigorous experimental studies of size-dependent optical and electronic properties. Beyond the basic scientific interest, PbX NQDs have already been successfully implemented in a range of prototype technologies including transistors,¹⁻⁶ photovoltaics,⁷⁻¹¹ photodetectors,¹²⁻¹⁴ light emitting diodes,^{15,16} and thermoelectrics.^{17,18} Despite these scientific and technological advances, significant questions concerning the electronic structure of PbX NQD persist.

The temperature coefficient and pressure coefficient of the energy gap of a semiconductor provides important experimental insights into the electronic structure of the material. In the case

of CdSe NQDs, high-pressure optical studies in diamond anvil cells have provided important understanding of the influence of quantum confinement on optical transitions.^{19,20} In contrast to most semiconductors from groups IV, II-VI, III-VI, and III-V, the energy gap of bulk PbX is known to exhibit a positive temperature coefficient (*i.e.* blue shift with increasing temperature) and a negative pressure coefficient (*i.e.* red-shift with increasing pressure).²¹ There have only been isolated reports of the pressure coefficients of PbSe NQD. Zhuravlev *et al.* reported pressure coefficients in the range of -47 to -56 meV/GPa for PbSe NQD with diameters tuned between 3 and 7 nm; the pressure coefficients were attributed predominantly to the bulk deformation potential with only a minor contribution due to changed in the quantum confinement energy.²² A more recent study by Pedrueza *et al.* interpreted the size-dependent pressure coefficient of the energy gap in PbSe NQD in context of pressure-dependent variation of the carrier effective mass.²³ Outstanding questions concerning the impact of quantum confinement effects on the pressure coefficient of PbX NQD motivate a closer look at the underlying structure-property relationships. Pressure coefficients of PbS NQD have, to the best of our knowledge, not been investigated. Moreover, changes in the electronic structure of PbS NQD accompanying the high-pressure B1-to-B16 (*i.e.*, rock-salt to orthorhombic) phase transition²⁴⁻²⁶ have not been reported.

We combined optical spectroscopy and synchrotron-based X-ray scattering of NQD colloidal suspensions in a diamond anvil cell (DAC) to simultaneously study isothermal pressure

coefficients of the electronic structure and crystal structure, respectively. We define the energy gap, E_g , as the energy of the lowest electron-hole pair transition. Our experimental approach allowed us to establish precise structure-property relationships including the pressure coefficient of the excitonic peak $\left(\frac{\partial E_g}{\partial P}\right)_T$ and the disappearance of the excitonic peak accompanying the phase transition from B1 to B16.

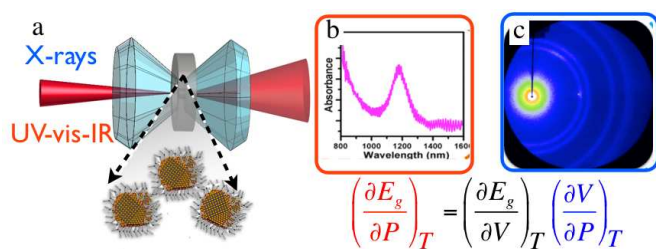


Figure 1. (a) Experimental setup for the combined characterization of crystal structure (X-ray scattering) and optical properties (optical absorbance). (b) Typical absorption spectrum illustrating the excitonic signatures (c) 2D X-ray scattering pattern at wide angles (WAXS) informs the nature of the atomic crystal and small angle scattering (SAXS) provides insight into inter-particle separation.

RESULTS AND DISCUSSION

PbS NQDs were synthesized by the hot-injection method and loaded into a diamond anvil cell for optical absorption and X-ray scattering experiments.²⁷ Experimental details are provided in the supporting information (SI). Parallel high-pressure measurements of the exciton peak energy and the crystal structure by optical absorption and X-ray scattering provide independent probes of $\left(\frac{\partial E_g}{\partial P}\right)_T$ and $\left(\frac{\partial V}{\partial P}\right)_T$, respectively (Figure 1). As detailed below, this approach allowed us to

study the relative contributions from the isothermal compressibility of the atomic lattice and the compression of the wave-function envelope of the NQD.

Figure 2 summarizes the pressure-dependent optical spectra of PbS NQDs. We probed three sizes of particles to determine the pressure coefficient in NQDs with varying extents of quantum confinement. The average NQD diameters of small ($3.0 \text{ nm} \pm 0.3 \text{ nm}$), medium ($3.7 \text{ nm} \pm 0.3 \text{ nm}$) and large ($6.7 \text{ nm} \pm 0.6 \text{ nm}$) were determined by statistical analysis of TEM images (Figure S1). At ambient pressure, the size-tuned excitonic peaks were measured to be 1766, 1090 and 839 meV, respectively. Pressure-dependent absorption spectra reveal two key trends: (i) the excitonic peak disappears as the NQD undergoes the pressure-induced transformation from rock-salt to orthorhombic crystal structure, (ii) the magnitude of the pressure-induced red shift of the excitonic peak decreases with decreasing NQD size. Below, we discuss both trends in detail.

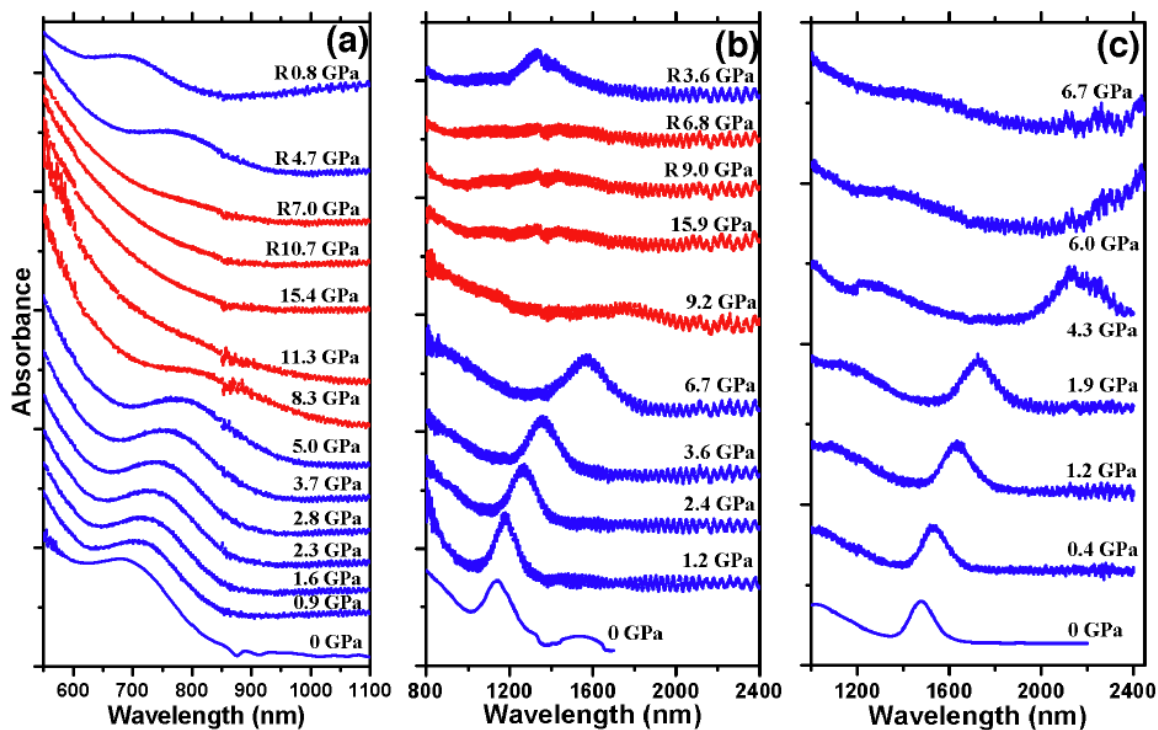


Figure 2. Optical absorbance spectra of PbS NQDs at various pressures. (a) Small, (b) Medium and (c) Large PbS NQDs. Blue and red curves represent low pressure rock salt and high pressure orthorhombic phases of PbS atomic lattice, respectively. The pressure for each spectrum is indicated; pressures during the return cycle to ambient pressure are denoted by R.

Azimuthally integrated wide-angle X-ray scattering (WAXS) of the three PbS NQD samples under elevated pressures are shown in Figure 3. The scattering data reveal that the crystal structure of PbS NQDs transforms from B1 (rock-salt) to B16 (orthorhombic) at pressures above ~ 7 GPa. WAXS peaks of small PbS NQDs are broadened due to their small size. The rock salt-to-orthorhombic phase transition²⁸ is indicated by the appearance of $\{110\}$ and $\{041\}/\{131\}$ peaks of the high-pressure orthorhombic lattice. The phase transition pressures of small, medium and large PbS are found to be around 8.5, 7.4 and 7.6 GPa respectively. The pressure-induced phase transition is reversible (see supporting information.)

The detailed crystal structures of intermediate phases in PbX remain controversial in the bulk material^{26,29,30} and have not been resolved in NQD. Generally, pressure induced phase transitions occur at higher pressures in NQD relative to the bulk counterpart.^{24,28,31,32} The optical absorption spectra of PbS NQD with rock-salt crystal structure (blue traces in Figure 2) show well defined excitonic peaks. At pressures above transition pressure, the excitonic peak disappears. The disappearance of the excitonic peak in PbS NQD near the transition pressure indicates a pronounced change in electronic structure. The transition from B1 to B16 crystal structure and the concomitant change in the excitonic absorption signature are reversible. The loss of excitonic peak cannot be observed in largest dots because transition is beyond the spectral limit of our

instrument (2400 nm). Figure 2a and 2b clearly show that the excitonic peak is recovered as the pressure is lowered, although the increased width of the excitonic peak after pressure cycling suggests that the NQD size distribution may have increased.

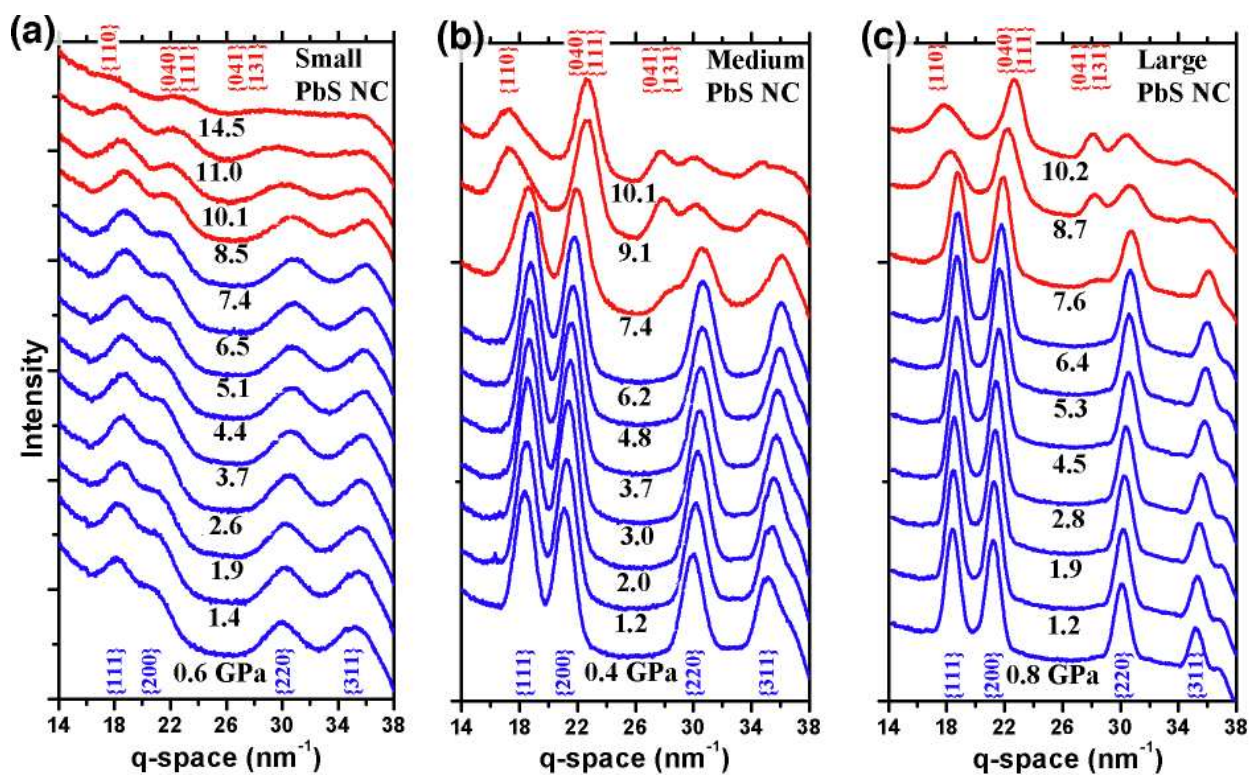


Figure 3. *in-situ* high-pressure WAXS spectra of (a) small, (b) medium and (c) large PbS NQDs. Blue and red curves represent low pressure rock salt and high pressure orthorhombic phases, respectively. The scattering peaks are labeled by their Miller indices.

Jiang *et al.* previously reported the change in electrical conductivity accompanying the high-pressure B1-to-B16 phase transition;³¹ the resistivity of PbS with 8 nm grain size was found to dramatically increase near the transition pressure and then exponentially decrease at higher pressures. Density functional theory calculations by Mehl and co-workers³³ have predicted the electronic structure of PbS with a transition to a metallic state; however, the predicted transition

pressure is two orders of magnitude above the experimental pressures tested in our study. The increasing peak width in the high-pressure WAXS data suggests that the crystallite size may have decreased, however this alone does not satisfactorily explain the reappearance of the excitonic peak as the pressure is returned to ambient. In light of the complex polymorphism of PbS crystals at high-pressure, further experimental and computational studies are required to improve understanding of the pressure-dependent electronic structure.

We now turn to discuss the pressure-coefficient of the excitonic peak in the ambient pressure, rock-salt, phase. At pressures ranging from ambient to ~5 GPa, the pressure coefficients, $\left(\frac{\partial E_g}{\partial P}\right)_T$, were determined from linear fits to be -40.6, -50.1 and -61.0 meV/GPa, for small, medium and large NQDs, respectively (see supporting information Figure S2). The direct relationship between the NQD size and the magnitude of the pressure coefficient is consistent with the trend of the bulk value which has been determined experimentally to be -91.0 meV/GPa³⁴ and theoretically to be -74.5 meV/GPa (density functional calculations),³³ -69 meV/GPa (augmented-plane-wave method),³⁵ and -54 meV/GPa (empirical pseudopotential method).³⁶ The decreasing magnitude of the pressure coefficient in smaller NQD is also consistent with previously reported temperature coefficients,³⁷ in the limit of atomic-like systems energy levels are expected to be independent of pressure and temperature.

To probe whether changes in the optical spectra are due to changes in interdot coupling, we measured interparticle spacing by small-angle X-ray scattering. Interdot coupling can significantly influence the electronic structure of the PbS NQD ensemble since the wave function of charge carriers extends significantly outside the boundary of the dot. Kim *et al.* previously reported optical properties of CdSe NQD assemblies as a function of pressure but found no significant signs of interdot coupling.¹⁹ Since interdot exchange coupling in PbX is more pronounced than in CdSe,³⁸ we need to consider how the external pressure influences the average separation between NQDs in the suspension. We monitored interdot spacing of the NQD suspension as a function of pressure using small-angle X-ray scattering (SAXS). SAXS data (see supporting information Figure S3-S4) show that the nearest-neighbor surface-to-surface separation between proximate NQD remains above 2.6, 3.8 and 3.5 nm for small, medium and large NQDs, respectively. Given the relatively large interparticle separations, we can confidently conclude that pressure-dependent changes in the exchange coupling are insignificant in the PbS NQDs suspensions studied here. Therefore, the observed change in the excitonic optical spectrum is predominantly due to changes within isolated particles detailed below.

We analyzed the pressure dependence of the NQD energy gap in terms of the relative contributions from the lattice and wave function envelope. The energy gap of semiconductor NQDs can be approximated by the model introduced by Brus.³⁹

$$E_g^{NQD} = E_g + \frac{\hbar^2 \pi^2}{2\mu R^2} - \frac{1.8e^2}{\epsilon_2 R} \quad (1)$$

where E_g is the energy gap of the corresponding bulk semiconductor. The second term represents the quantum confinement as a function of NQD radius, R , and reduced effective mass, μ , of the semiconductor. The third term represents the Coulombic attraction between the electron and the hole, and ϵ_2 is the dielectric constant of the NQD. The original Brus model also included a fourth term to account for dielectric solvation energy loss; this term is comparatively small in magnitude and can be neglected in the analysis of the pressure-dependent energy gap.

The pressure derivative of the energy gap (eqn.1) can be expressed as:

$$\left(\frac{\partial E_g^{NQD}}{\partial P}\right)_T = \left(\frac{\partial E_g}{\partial P}\right)_T + \frac{\hbar^2 \pi^2}{2} \frac{\partial}{\partial P} \left(\frac{1}{\mu R^2}\right)_T - \frac{1.8e^2}{\epsilon_2} \frac{\partial}{\partial P} \left(\frac{1}{R}\right)_T \quad (2)$$

The first term accounts for the compressibility of the bulk lattice (*i.e.* $\left(\frac{\partial E_g^b}{\partial a}\right)_T \left(\frac{\partial a}{\partial P}\right)_T$). The quantum-confinement and the Coulombic terms reflect the pressure dependence of the wavefunction envelope and involve the change in NQD radius with pressure, which can be related to the bulk modulus, B_o , as $\left(\frac{\partial R}{\partial P}\right)_T = \frac{-R_o}{3B_0}$ (see SI for details).

One can consider modeling the pressure dependency of the NQD energy gap in terms of the corresponding parameters of bulk PbS, namely, the pressure coefficient of

$$\left(\frac{\partial E_g^b}{\partial P}\right)_T = -91 \text{ meV / GPa}^{34} \text{ and bulk modulus } (B_0=53 \text{ GPa})^{25} \text{ and a reduced effective mass of}$$

0.0387 m_0 . This basic model is inconsistent with the experimentally observed trends and significantly overestimates the size-dependency of the pressure coefficient. A previous study of PbSe NQD by Pedrueza *et al.*²³ considered a pressure dependent effective mass to account for the departure from the basic model. Our approach, detailed below, focused on the size dependence of the bulk moduli that were independently determined from X-ray scattering structure analysis. Additional calculations provided in the supporting information show that allowing for the effective mass as a pressure-dependent parameter does not significantly improve the fit to our experimental data on PbS NQD.

The bulk modulus has significant impact on both the compressibility of the atomic lattice and the wave function envelope. To test this hypothesis and to rigorously relate the pressure-dependent NQD radius and energy gap, we measured the size-dependent bulk modulus from X-ray scattering analysis of NQD lattice constant, a , as a function of dot size and applied pressure. We fitted variable-pressure wide-angle X-ray scattering data to the pressure-volume relationship of the Vinet equation of state (see SI for details):

$$P = 3B_0 v^{-2/3} [1 - v^{1/3}] \exp\{1.5(B_0' - 1)[1 - v^{1/3}]\} \quad (2)$$

where $B_0 = B|_{P=0}$ is the bulk modulus under ambient pressure, $B'_0 = dB/dP|_{P=0}$ is the initial slope, and v is the unit cell volume of the NQD crystal lattice. In this study, B'_0 is fixed at 4.0 for all samples.^{32,33}

Table 1 summarizes the size-dependent bulk moduli of PbS NQD derived from X-ray scattering measurements (Figure 4a) and fits to the Vinet equation of state. (Details in SI) The data reveal two important features: (1) the bulk moduli of PbS NQDs are larger than the corresponding literature value of bulk PbS and (2) for the NQD sizes studied in our work, the bulk modulus increases with decreasing particle size. A comprehensive description of the bulk modulus of PbS nanostructures as a function of size, shape and surface composition is beyond the scope of this paper and will be detailed in a future report. In the following section, we demonstrate that for PbS NQDs, the detailed size-dependence of B_0 has important implications on the optical/electronic properties of PbS NQD.

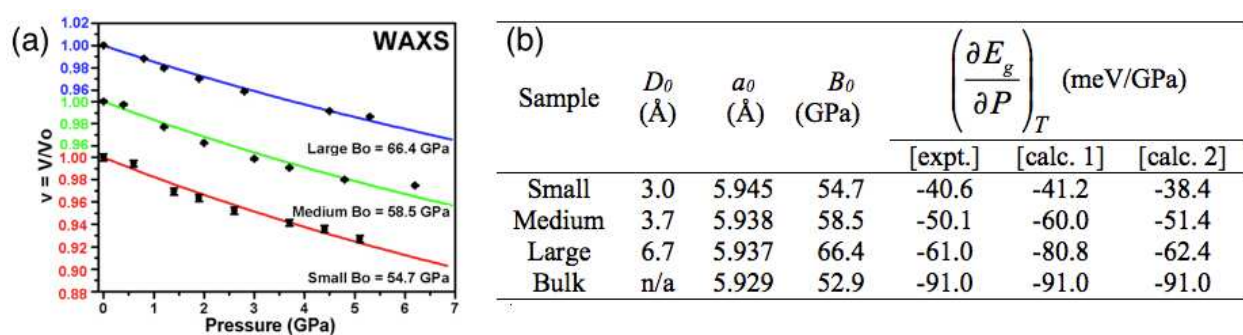


Figure 4. *in-situ* high-pressure X-ray scattering measurements on small (red), medium (green) and large (blue) (a) normalized atomic unit cell volume of PbS NQD cores measured by WAXS. (b) summary of experimental values of diameter (D_0), ambient pressure lattice constant (a_0), bulk moduli (B_0) and pressure variation of energy gap of PbS NQDs of different sizes compared with calculated values based on the basic model [calc. 1] and the detailed model [calc. 2].

Accounting for the size-dependent bulk modulus into the model of the pressure-dependent exciton peak energy (eqn.2) yields a significantly improved fit to the experimentally observed trends (see Figure S5). We note that the size-dependent bulk modulus not only affects the quantum confinement and Coulombic terms, but also impacts the bulk pressure coefficient (first term in eqn.2); a detailed derivation is provided in the SI. Table 1 compares the relative magnitudes of the quantum confinement and Coulombic terms calculated by the detailed model. The pressure-dependent excitonic peak is more strongly influenced by the quantum confinement term while the Coulombic term has negligible impact.

| Sample | R_0 (nm) | $\left(\frac{\partial E_g^b}{\partial a}\right)_T \left(\frac{\partial a}{\partial P}\right)_T$ | $\left(\frac{\hbar^2 \pi^2}{3B_o \mu R^2}\right)$ | $\left(\frac{1.8e^2}{3B_o \epsilon_2 R}\right)$ | $\left(\frac{\partial E_g}{\partial P}\right)_T$ (calc.) | $\left(\frac{\partial E_g}{\partial P}\right)_T$ (measured) |
|--------|---------------|---|---|---|---|--|
| S | 1.5 | -88.2 | 50.4 | -0.59 | -38.4 | -40.6 |
| M | 1.9 | -82.4 | 31.4 | -0.43 | -51.4 | -50.1 |
| L | 3.3 | -72.6 | 10.4 | -0.24 | -62.4 | -61.0 |
| Bulk | n/a | -91.0 | 0 | 0 | -91.0 | n/a |

Table 1. Comparison of bulk, quantum confinement and Coulombic terms in eqn. 2 calculated by the detailed model. Unit for all terms is meV/GPa.

Conclusion

In summary, we present *in-situ* optical absorption and X-ray scattering measurements to probe the pressure-dependent shift in the excitonic absorption peak of colloidal PbS NQD. The excitonic peak shifts towards the red with increasing pressure and disappears at a pressure

corresponding to the phase transition from rock-salt to orthorhombic crystal structure. The pressure coefficient of energy gap $\left(\frac{\partial E_g}{\partial P}\right)_T$ strongly depends on NQD size: the smaller the NQD is, the less sensitive its energy gap is to pressure. The combination of optical spectroscopy and structural information of NQDs measured by *in-situ* high-pressure WAXS, allowed us to establish a model for the pressure coefficient of the excitonic peak. The detailed model is in good agreement with experimentally observed trends and provides quantitative insights into the contributions to the size-dependence. Our calculations reveal that the size-dependence is mainly caused by the size-dependent quantum confinement energy, the compressibility of PbS NQD cores and less importantly by the exciton potential energy.

Acknowledgement

X-ray scattering experiments were conducted at the Cornell High Energy Synchrotron Source (CHESS), which is supported by the National Science Foundation and the National Institutes of Health/National Institute of General Medical Sciences under NSF award DMR-0936384. KB was supported by NSF-DMR 1056943. FW and TH acknowledge support from U.S. Department of Energy, Office of Basic Energy Sciences, Division of Materials Sciences and Engineering under Award DE-SC0006647.

REFERENCES

1. D. V. Talapin and C. B. Murray, *Science*, 2005, **310**, 86.
2. D. V. Talapin, J.-S. Lee, M. V. Kovalenko, and E. V. Shevchenko, *Chem Rev*, 2010, **110**, 389–458.
3. W.-K. Koh, A. Y. Kuposov, J. T. Stewart, B. N. Pal, I. Robel, J. M. Pietryga, and V. I. Klimov, *Sci. Rep.*, 2013, **3**.
4. T. Hanrath, *Journal of Vacuum Science & Technology, A: Vacuum, Surfaces, and Films*, 2012, **30**, 030802.
5. S. Z. Bisri, C. Piliego, M. Yarema, W. Heiss, and M. A. Loi, *Adv Mater*, 2013, **25**, 4309–4314.
6. M. S. Kang, J. Lee, D. J. Norris, and C. D. Frisbie, *Nano Lett*, 2009, **16**, 3848–3852.
7. J. J. Choi, Y.-F. Lim, M. B. Santiago-Berrios, M. Oh, B.-R. Hyun, L. Sung, A. C. Bartnik, A. Goedhart, G. G. Malliaras, H. D. Abruna, F. W. Wise, and T. Hanrath, *Nano Lett*, 2009, **9**, 3749–3755.
8. J. Gao, C. L. Perkins, J. M. Luther, M. C. Hanna, H.-Y. Chen, O. E. Semonin, A. J. Nozik, R. J. Ellingson, and M. C. Beard, *Nano Lett*, 2011, **11**, 3263–3266.
9. L. Etgar, T. Moehl, S. Gabriel, S. G. Hickey, A. Eychmuller, and M. Gratzel, *ACS Nano*, 2012, **6**, 3092–3099.
10. J. Tang and E. H. Sargent, *Adv Mater*, 2010, **23**, 12–29.
11. K. S. Leschkies, T. J. Beatty, M. S. Kang, D. J. Norris, and E. S. Aydil, *ACS Nano*, 2009, **3**, 3638–3648.
12. G. Konstantatos, I. Howard, A. Fischer, S. Hoogland, J. Clifford, E. Klem, L. Levina, and E. Sargent, *Nature*, 2006, **442**, 180–183.
13. G. Konstantatos and E. H. Sargent, *Appl Phys Lett*, 2007, **91**, 173505.
14. K. K. Manga, J. Wang, M. Lin, J. Zhang, M. Nesladek, V. Nalla, W. Ji, and K. P. Loh, *Adv Mater*, 2012, **24**, 1697–1702.
15. L. Sun, J. J. Choi, D. Stachnik, A. C. Bartnik, B. R. Hyun, G. G. Malliaras, T. Hanrath, and F. W. Wise, *Nature Nanotech*, 2012, **7**, 369–373.
16. X. Ma, F. Xu, J. Benavides, and S. G. Cloutier, *Organic Electronics*, 2012, **13**, 525–531.
17. M. Ibáñez, R. Zamani, S. Gorsse, J. Fan, S. Ortega, D. Cadavid, J. R. Morante, J. Arbiol, and A. Cabot, *ACS Nano*, 2013, **7**, 2573–2586.
18. R. Y. Wang, J. P. Feser, J.-S. Lee, D. V. Talapin, R. Segalman, and A. Majumdar, *Nano Lett*, 2008, **8**, 2283–2288.
19. B. Kim, M. Islam, L. Brus, and I. Herman, *J Appl Phys*, 2001, **89**, 8127–8140.
20. S. Tolbert, A. Herhold, C. Johnson, and A. Alivisatos, *Phys Rev Lett*, 2011, **73**, 3266–3269.
21. M. Schlüter, G. Martinez, and M. L. Cohen, *Phys Rev B*, 1975, **12**, 650.
22. K. K. Zhuravlev, J. M. Pietryga, R. K. Sander, and R. D. Schaller, *Appl Phys Lett*, 2007, **90**, 043110.
23. E. Pedrueza, A. Segura, R. Abargues, J. B. Bailach, J. C. Chervin, and J. P. Martínez-

- Pastor, *Nanotechnology*, 2013, **24**, 205701.
24. S. B. Qadri, J. Yang, B. R. Ratna, E. F. Skelton, and J. Z. Hu, *Appl Phys Lett*, 1996, **69**, 2205–2207.
 25. K. Knorr, L. Ehm, M. Hytha, B. Winkler, and W. Depmeier, *European Physical Journal B*, 2003, **31**, 297–303.
 26. A. Grzechnik and K. Friese, *Journal of Physics: Condensed Matter*, 2010, **22**, 095402.
 27. Z. Wang, O. Chen, C. Y. Cao, K. Finkelstein, D.-M. Smilgies, X. Lu, and W. A. Bassett, *Review of Scientific Instruments*, 2010, **81**, 093902.
 28. K. Bian, Z. Wang, and T. Hanrath, *J Am Chem Soc*, 2012, **134**, 10787–10790.
 29. T. Chattopadhyay, H. G. Von Schnering, W. A. Grosshans, and W. B. Holzapfel, *Physica B+ C*, 1986, **139**, 356–360.
 30. R. Ahuja, *Phys. Stat. Sol (b)*, 2003, **235**, 341–347.
 31. J. Z. Jiang, L. Gerward, R. Secco, D. Frost, J. S. Olsen, and J. Truckenbrodt, *J Appl Phys*, 2000, **87**, 2658.
 32. P. Podsiadlo, B. Lee, V. B. Prakapenka, G. V. Krylova, R. D. Schaller, A. Demortiere, and E. V. Shevchenko, *Nano Lett*, 2011, **11**, 579–588.
 33. M. Lach-hab, D. A. Papaconstantopoulos, and M. J. Mehl, *Journal of Physics and Chemistry of Solids*, 2002, **63**, 833–841.
 34. O. Madelung, M. Schulz, H. Weiss (Eds.), *Numerical Data and Functional Relationships in Science and Technology Landolt-Bornstein, New Series*, vol. 17, Springer, Berlin, 1983.
 35. S. Rabbii, *Physical Review*, 1968, **167**, 801.
 36. P. J. Lin and L. Kleinman, *Physical Review*, 1966, **142**, 478.
 37. A. Olkhovets, R. C. Hsu, A. Lipovskii, and F. Wise, *Phys Rev Lett*, 1998, **81**, 3539–3542.
 38. K. Overgaag, P. Liljeroth, B. Grandidier, and D. Vanmaekelbergh, *ACS Nano*, 2008, **2**, 600–606.
 39. L. E. Brus, *J Chem Phys*, 1984, **79**, 4403–4412.

TOC Figure

